Effect of elastic strain energy on self-organized pattern formation

E Pan[1]*, **R Zhu**[1], and **P W Chung**[2]
[1]Department of Civil Engineering, University of Akron, Akron, Ohio, USA
[2]US Army Research Laboratory, Aberdeen Proving Ground, Maryland, USA

The manuscript was received on 23 February 2005 and was accepted after revision for publication on 14 April 2005.

DOI: 10.1243/174034905X47385

Abstract: This paper studies the growth of self-organized quantum dots in strained semiconductors in the Stranski–Krastanov growth mode using the kinetic Monte Carlo simulation method. The four nearest and four next nearest neighbours of each atom in the square lattice grid with a periodic boundary condition are considered in the calculation of the binding energy among atoms. The elastic strain energy is accurately evaluated by the rigorous point eigenstrain half-space Green's function and is incorporated for the first time into the kinetic Monte Carlo model. The set of relevant growth parameters such as growth temperature, surface coverage, flux rate, and growth interruption time, is investigated and optimal values are identified. It is shown clearly that when the long-range elastic strain energy is included in the simulation, uniform size and ordered spatial distribution can be achieved. Furthermore, the growth of stacked quantum dot layers is also simulated briefly and vertical alignment is observed that could lead to progressively uniform island size and spatial ordering.

Keywords: quantum dot, self-organization, Stranski–Krastanov growth, elastic strain energy, strained semiconductor, kinetic Monte Carlo, Green's function

1 INTRODUCTION

Nanoscale quantum dot (QD) superlattices have been intensively studied in recent years owing to their confined optical and electronic properties with potential applications in optoelectronics and semiconductor devices [**1**, **2**]. Self-organized growth is a promising way to grow QD islands with uniform size and ordered spatial distribution. However, it is still very challenging to grow high-density and dislocation-free QD layers self-organizationally, even under the Stranski–Krastanov growth model [**3**–**5**]. Since, experimentally, this trial-and-error growth approach could be very expensive and time-consuming, numerical simulation methods can be utilized to provide important information and guidance to experimentalists. As the self-organized QD growth is a competitive balance between the binding and thermal energies, involving atom deposition and diffusion, certain kinetic Monte Carlo (KMC) models have been proposed to simulate the process numerically [**6**, **7**]. It was observed by Schöll and Bose [**8**] and Elsholz *et al.* [**9**], among others, that a probability governed by the Arrhenius law including the sole atomic binding energy would result in the Ostwald ripening phenomenon in the KMC model. However, when the long-range elastic strain energy is considered, cooperative growth, where larger islands lose some atoms to smaller ones, could be achieved.

Long-range strain-controlled QD growth mechanisms have been investigated, including those considering the elastic energy induced by the lattice misfit as the sole dominant parameter in the self-organized growth [**5**]. This elastic energy due to the misfit lattice has also been utilized to explain the correlation and anticorrelation features observed in the layer-by-layer QD growth [**4**, **10**, **11**]. Motivated perhaps by these observations, the long-range elastic strain energy was recently introduced into the Arrhenius law by Meixner *et al.* [**7**], based on the point/line force Green's function solution, and interesting features differing from those without elastic strain were observed. However, it is understood that during the epitaxial growth the strain energy is due

*Corresponding author: Department of Civil Engineering, University of Akron, Akron, OH 44325-3905, USA. email: pan2@uakron.edu

to the lattice misfit (eigenstrain) between the substrate and the adatoms rather than the point/line force, and thus the corresponding Green's function due to the point eigenstrain should be employed in order to simulate correctly the growth process.

In this article, a KMC model is developed that includes the correct and accurate elastic strain energy due to the lattice-misfit eigenstrain [**12**, **13**]. The semiconductor material is assumed to be GaAs (001), and the strain energy is calculated as an integration of the point eigenstrain half-space Green's function [**12–14**]. This strain energy modified KMC model was used to study the effect of growth parameters on the QD growth pattern. These parameters include temperature T, flux rate F to the surface during deposition, surface coverage c, and growth interruption time t_i [**7**, **15–17**]. The simulated island ordering and narrow size distribution are discussed and optimized growth parameters are identified.

In order to study the growth of stacked QD layers or the so-called superlattice structure, the self-organized growth model is briefly extended from the horizontal plane to the third dimension, which is the growth direction. It is well known that the growth parameters can greatly affect the QD structure [**18**, **19**] and the strain energy generated by the buried QDs can induce spatial correlations between islands at the surface and those below [**20**]. The strain field on the surface generated by the QDs below contributes to the QD island spatial ordering on the surface [**5**, **21**, **22**]. A thermodynamic equilibrium theory including the elastic strain has shown that vertical correlations and anticorrelations in multilayered superlattices are functions of layer thickness [**23**], but the effect of kinetics in these stacks is not well understood [**11**]. Therefore, this paper also presents KMC simulation incorporating the strain fields on the topmost layer and the layers below, including also the interaction among them. For a three-layered QD structure, the simulated results show that, with increasing layer number, uniform island size and ordered spatial distribution could be achieved.

2 MODELLING APPROACH

2.1 Atomic hopping probability

This paper presents simulation based on the activated atom diffusion incorporating the local elastic strain energy field. The hopping probability of an atom from one lattice site to a nearest or next nearest neighbour site in the horizontal (x, y) plane is governed by the Arrhenius law [**24**, **25**]

$$p = \nu_0 \exp\left(-\frac{E_s + E_n - E_{str}(x,y)}{k_B T}\right) \quad (1)$$

where ν_0 is the attempt frequency ($= 10^{13}\,s^{-1}$), T the temperature, and k_B the Boltzmann's constant. Also in equation (1), E_s and E_n are the binding energies to the surface and to the neighbouring atoms respectively. Finally, $E_{str}(x, y)$, as a function of the plane coordinates (x, y), is the energy correction from the long-range strain field due to the lattice misfit between the substrate and the deposited material. While the binding energy to the surface is assumed to be constant in this article (actually, $E_s = 1.3\,eV$), that to the neighbouring atoms, i.e. E_n, is evaluated as below.

It is assumed that the strength of a single nearest neighbour bond is E_b ($= 0.3\,eV$), and it is reduced by a factor $\alpha(= 1/\sqrt{2})$ for the next nearest neighbours. To evaluate the diffusion barrier, the binding energy at the site S_0, where the diffusing atom is located, is calculated to be

$$E_{s_0} = nE_b + \alpha m E_b \quad (2)$$

with $n \leqslant 4$ and $m \leqslant 4$ being, respectively, the number of nearest and next nearest atoms. Similarly, for the site S_1 to where the atom is going to hop

$$E_{s_1} = g(n' E_b + \alpha m' E_b) \quad (3)$$

where $n' \leqslant 4$ and $m' \leqslant 4$ are respectively the number of nearest and next nearest atoms at the new site S_1, and g ($= 0.2$) describes the coupling between adjacent lattice sites. Therefore, the overall binding energy E_n caused by the neighbour interaction for a diffusion process from site S_0 to site S_1 is given by the difference of the binding energies at the corresponding lattice sites [**7**, **11**]

$$E_n = (n - gn')E_b + (m - gm')\alpha E_b \quad (4)$$

Thus, for diffusion along step edges or around corners, the hopping probability is slightly enhanced.

2.2 Off, edge, and corner diffusion

There are three different kinds of diffusion for each atom in the periodic lattice area: off, edge, and corner diffusions (Fig. 1). 'Off' diffusion means an atom diffuses away from its neighbours. The diffusion

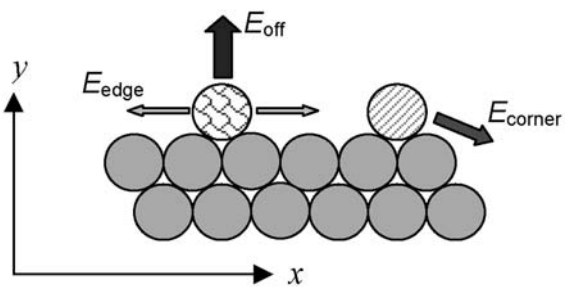

Fig. 1 Schematic of off, edge, and corner diffusions on the horizontal (x, y) plane

barrier for 'off' diffusion is increased by (next) nearest neighbour bonds E_n. 'Edge' diffusion means that an atom diffuses along the edge of an island, and some of the bonds to the (next) nearest neighbour stay intact. Consequently, the energy barrier for diffusion along an edge E_{edge} will generally be smaller than E_{off}. 'Corner' diffusion means that an atom diffuses around the corner of some islands. For 'corner' diffusion, the number of intact bonds to nearest and next nearest neighbours is smaller than that of 'edge' diffusion. Thus, in summary, the barrier relation among 'off', 'corner', and 'edge' atoms is $E_{off} > E_{corner} > E_{edge}$.

2.3 Incorporation of the strain energy field

As pointed out in the introduction, while the strain energy field is very important in self-organized growth, it needs to be accurately calculated. In other words, for the strained semiconductor structure, use should be made of the strain energy due to the point eigenstrain, instead of that due to the point/line force. The correct formulation for the calculation of the strain energy is strictly presented below, leaving the details in Appendix 2 for reference.

Within the framework of continuum elasticity, the elastic strain induced by an island of atoms can be obtained using the Green's function solution for the anisotropic semiconductor substrate [**12**, **13**]. Assuming that there is a point misfit strain (or eigenstrain) γ^*_{ij} (due to the misfit lattice difference) at $\boldsymbol{x}$, then the induced elastic strain at $\boldsymbol{y}$ can be found as

$$\gamma_{kp}(\boldsymbol{y};\boldsymbol{x}) = \tfrac{1}{2}\gamma^*_{lm}[\sigma^k_{ml,p_y}(\boldsymbol{x};\boldsymbol{y}) + \sigma^p_{ml,k_y}(\boldsymbol{x};\boldsymbol{y})] \tag{5}$$

where the superscript k or p (= 1, 2, 3) on the right-hand side of equation (5) indicates the direction of the point force, and the subscript prime followed by p_y or k_y in the stress component σ_{ml} denotes the derivative of Green's stress. With the elastic strain (5) due to a point misfit lattice, the strain energy at $\boldsymbol{y}$ due to an island of atoms with area A (with unit thickness in the out-of-plane z direction) at variable $\boldsymbol{x}$ can be calculated as (see also Appendix 2 for detail)

$$E_{str}(\boldsymbol{y}) = \frac{1}{2} C_{ijkl} \iint_A \gamma_{ij}(\boldsymbol{y};\boldsymbol{x})\gamma_{kl}(\boldsymbol{y};\boldsymbol{x})\,\mathrm{d}A(\boldsymbol{x}) \tag{6}$$

where C_{ijkl} is the elastic stiffness tensor. In the following calculation, it is assumed that the misfit strain is hydrostatic, i.e. $\gamma^*_{ij} = \gamma^*\delta_{ij}$ with $\gamma^* = 0.07$. The non-zero elastic coefficients for GaAs (001) [**13**] are taken to be $C_{11} = 118$, $C_{12} = 54$, and $C_{44} = 59$ (10^9 N/m^2).

2.4 Kinetic Monte Carlo algorithm

The simulation routine is based on a continuous time Monte Carlo scheme. The BKL algorithm named after Bortz, Kalos, and Lebowitz [**26**] is very efficient for the problem at hand, since the independence of a particular timescale is of great advantage in simulating surface diffusion.

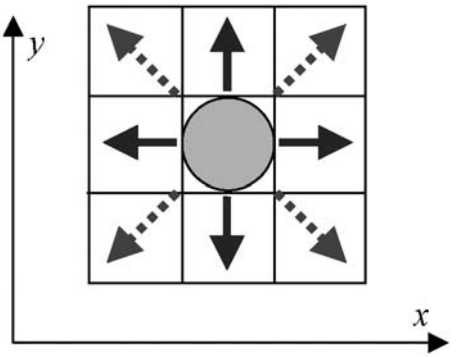

Fig. 2 Schematic of nearest (x and y directions in solid lines) and next nearest (diagonal directions in dashed lines) neighbour positions of each atom in the horizontal (x, y) plane

In the present program, atom diffusion processes are simulated one by one. The principal course of the simulated diffusion is the same and can be sketched in the following. Each atom at most has four possible nearest and four possible next nearest diffusion positions (Fig. 2), or four nearest and four next nearest neighbours. Every possible diffusion step of a given atom is done by evaluating the probability p from equation (1). These eight possible diffusion probabilities to nearest and next nearest neighbour positions are stored and added to find the total diffusion probability, p_{atom}, for the atom. The total probability that anything might happen at all is then given by adding all the probability p_{atom} to obtain p_{total}. During the simulation, an atom is randomly chosen to move across the surface by hopping to the nearest or next nearest lattice site. The key is to assign a proper weight to each atom to be chosen, considering that different atoms contribute differently to the overall probability p_{total} (see, for example, equations (1) and (4)). From the eight possible diffusion processes of the selected atom, one is chosen in accordance with its likelihood and executed. The corresponding time interval Δt is calculated and added to the elapsed simulation time.

The movement of an atom also alters the diffusion barriers for the neighbouring atoms in the previous neighbourhood as well as in the new one. As such, the moving atom and all the atoms in its surrounding area have to be recalculated to obtain the new diffusion probabilities. As for the strain energy, strictly speaking, it would have to be calculated at each step. However, since the strain evaluation is a lengthy procedure and the strain only slightly changes with the motion of a single atom, it turns out that it is

optimal to calculate the strain field at every 2500 jump steps (the present examples show that, for steps between 1000 and 3500, the simulation patterns are nearly identical; in consideration of both efficiency and accuracy, strain energy is calculated in this paper at every 2500 steps). To speed up further the computation, the strain energy calculation does not extend over the whole system but only over a circular area of a given radius r around the point where the strain is to be evaluated, due to the rapid decay of this field. In the following examples, such a radius r is taken to be 30 lattice grids [**8**]. The detailed simulation steps are listed in Appendix 3.

3 EFFECT OF GROWTH PARAMETERS ON ISLAND SIZE AND ORDERING

For most electronic and optical applications that include active QD layers, it is important to have many equally shaped dots. Unfortunately, the problem of generating self-organized QD patterns cannot be solved in a straightforward manner. Even though Stranski–Krastanov growth is known to be suitable for self-organized QD growth, there are many parameters that can considerably influence the growth result. Some of the relevant parameters are temperature T, flux rate F, coverage c, and interruption time t_i. There follows, a discussion of the effect of these parameters on the island growth of material GaAs (001) on a 200×200 lattice size with a periodic boundary condition and with strain energy for all atoms being updated at every 2500 hopping steps.

3.1 With and without strain energy

The nearest and next nearest neighbour binding energies contribute to the shape of the compact islands; however, the island–island interaction is very weak without strain energy. As the strain energy is calculated based on the point eigenstrain Green's function, it is expected that the absolute value of strain energy is the largest at the boundary area of an island, and with increasing distance away from the island it decays rapidly [**12**, **13**, **20**]. Thus, the interaction among islands could lead to spatial ordering due to the long-range strain field. This is why, without elastic strain energy, neither ordered size nor ordered spatial distribution can be observed, and Ostwald ripening would be expected [**9**, **27**]. To demonstrate the importance of strain energy, island ordering of adatoms with and without elastic strain energy is shown in Fig. 3 for simulation parameters $T = 750\,\mathrm{K}$, $F = 1.0\,\mathrm{Ml/s}$, $c = 20$ per cent, and $t_i = 200\,\mathrm{s}$.

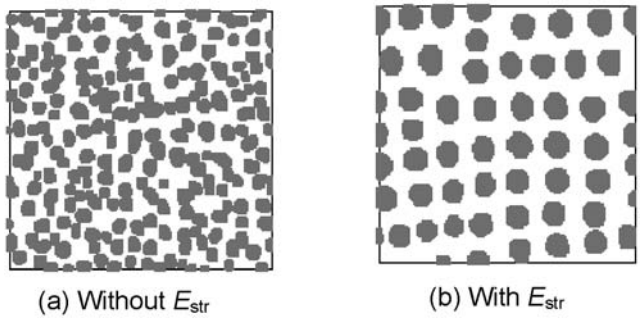

Fig. 3 Island ordering of adatoms without (a) and with (b) elastic strain energy. Simulation parameters are $T = 750\,\mathrm{K}$, $F = 1.0\,\mathrm{Ml/s}$, $c = 20$ per cent, and $t_i = 200\,\mathrm{s}$ on a 200×200 grid. The strain energy field is updated at every 2500 steps in (b)

From Fig. 3 it is clear that, without considering the elastic strain energy, the nearest and next nearest neighbour binding energy can still lead to isolated islands but no ordered island size and spatial distribution can be observed (Fig. 3(a)). However, when the strain energy is included, all the islands have approximately the same size and the distance between any two islands is also about the same, showing clearly ordered island size and spatial distribution (Fig. 3(b)).

3.2 Temperature T

The growth temperature T can greatly affect the simulation result. If the temperature T is too low, the deposited atoms will just stick to the surface without enough thermal energy to diffuse (Fig. 4(a)). In this case, of course, no self-organization is expected to happen. If, on the other hand, the temperature is too high, then interatomic bonds are too weak to be broken and an ensemble of monomers and small polymers with atoms performing random walks over the surface would be expected. For this situation, large islands are inherently unstable. Therefore, only for certain temperatures can the self-organization be effective.

The temperature dependence of the average island size is shown in Fig. 4 for fixed flux rate $F = 1\,\mathrm{Ml/s}$ and coverage $c = 20$ per cent. Here, deposition stops after 0.2 s of simulation time and the growth interruption time t_i is 200 s. It can be seen from Fig. 4 that, starting from $T = 550\,\mathrm{K}$, the higher the temperature, the larger is the average island size. Correspondingly, the islands become more and more ordered (Figs 4(a) to (d)). However, when the temperature is equal to, or higher than, 850 K, the thermal energy dominates, and the order of island arrays breaks down with increasing temperature (Figs 4(e) to (f)). Therefore, the optimal temperatures for this testing model are values around 800 K.

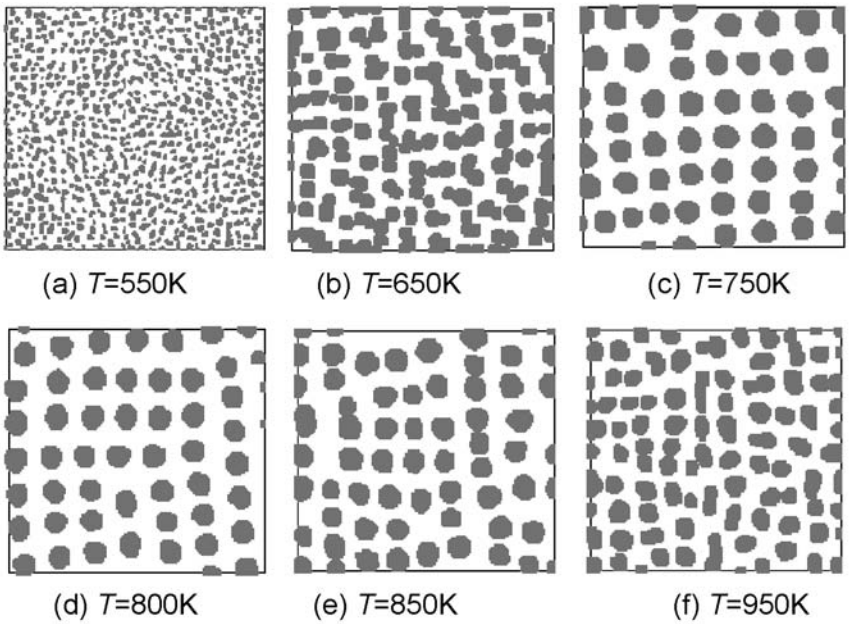

Fig. 4 Atom island ordering under different temperatures (T is 550 K in (a), 650 K in (b), 750 K in (c), 800 K in (d), 850 K in (e), and 950 K in (f)). Simulation parameters are $F = 1.0$ Ml/s, $c = 20$ per cent, and $t_i = 200$ s on a 200×200 grid. The strain energy field is updated every 2500 steps

3.3 Flux rate F

The flux rate F is defined as the deposition of material on the surface per unit time, and it is therefore a measurement of how fast the material is deposited on the surface. It does not include any equation concerning processes connected with self-organization and influences only indirectly the kinetics of growth by indicating the density of atoms on the surface and the nucleation rate of islands. Since flux is present during the time of deposition only, it might be assumed that it is less important during growth interruption. However, different values of flux rate can lead to significant differences in the surface morphology at the end of deposition. Under low flux rate (e.g. $F = 0.01$ Ml/s in Fig. 5(c)), the system will have enough time during the deposition process to come close to an equilibrium size distribution with large-size islands. On the other hand, a small-size island distribution is associated with a high flux rate. In other words, in general, the lower the flux rate, the larger is the equilibrium island size, as illustrated in Fig. 5 for different flux rates with fixed temperature $T = 700$ K, coverage $c = 20$ per cent, and interruption time $t_i = 200$ s. Note that, to highlight the effect of the flux rate, the strain energy field is not included in this simulation.

3.4 Surface coverage c

The surface coverage c describes how much material is deposited on the surface. This parameter certainly has an important effect on size distribution as islands of equilibrium size cannot be expected if there is not enough deposited material on the surface. On the

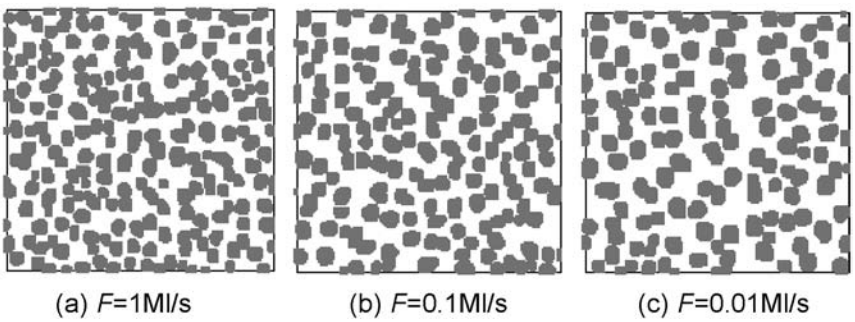

Fig. 5 Island ordering of atoms under different flux rates ($F = 1$ Ml/s in (a), $F = 0.1$ Ml/s in (b), and $F = 0.01$ Ml/s in (c)). Simulation parameters are $T = 700$ K, $c = 20$ per cent, and $t_i = 200$ s on a 200×200 grid. Deposition stops after 0.2 s in (a), 2 s in (b), and 20 s in (c), and the strain energy field is not included for simplicity

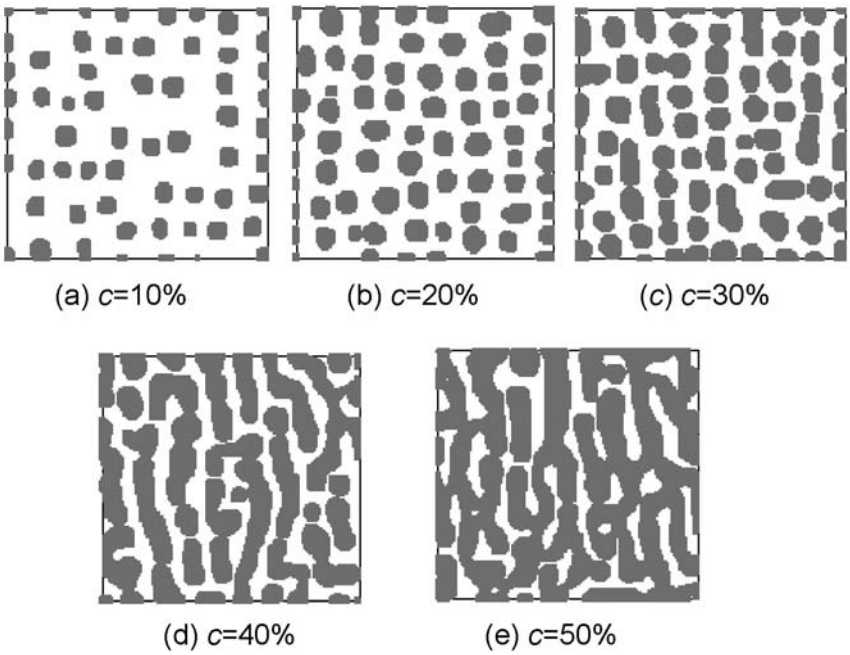

Fig. 6 Atom island ordering with coverage c increasing from 10 to 50 per cent in (a) to (f). Simulation parameters are $T = 700\,\mathrm{K}$, $F = 1.0\,\mathrm{Ml/s}$, and $t_\mathrm{i} = 200\,\mathrm{s}$ on a 200×200 grid. The strain energy field is updated every 2500 steps

other hand, if too much material is transported to the surface, too small a distance between islands makes the formation of isolated islands impossible (e.g. Figs 6(d) and (e)). For coverage below certain critical coverage c_c, the growth is mainly kinetically controlled. In other words, the island size distribution is mostly controlled by the variation in coverage and an increase in the average island size would be expected with increasing coverage (Figs 6(a) to (c)). Under this condition, every island collects atoms from its immediate vicinity without any considerable exchange of material among islands, and its size is directly determined by the amount of deposited material around the island.

For temperature $T = 700\,\mathrm{K}$, flux rate $F = 1\,\mathrm{Ml/s}$, and interruption time $t_\mathrm{i} = 100\,\mathrm{s}$, the simulated results on the 200×200 grid with different coverage are plotted in Fig. 6. From the results it can be seen that, with increasing coverage from 10 to 30 per cent, the average island size becomes larger and larger. However, when the coverage is larger than 30 per cent, isolated islands cannot be easily observed. Therefore, the critical surface coverage, c_c, is somewhere between 20 and 30 per cent.

3.5 Growth interruption time t_i

Another important factor to influence the growth result is the time between the end of deposition and the capping of the QD layer with another material, the so-called growth interruption time, while the time from the very beginning to the end of simulation is named the total simulation time t ($= t_\mathrm{i} +$ deposit time). It is known that growth interruption affects the crystal surface dramatically and the results before and after the interruption can be very different [**16**]. Furthermore, during growth interruption, the atoms can move to energetically favourable positions and approach thermodynamic equilibrium. Since there is a striking difference between the kinetically controlled growth and the thermodynamically dominated size distribution, the effect of growth interruption time can be dramatic.

For temperature $T = 750\,\mathrm{K}$, flux rate $F = 1\,\mathrm{Ml/s}$, and coverage $c = 20$ per cent on the grid of 200×200, the simulation results with different growth interruption times are shown in Figs 7(a) to (f). It is clear that with increasing t_i, the island size increases. At about $t_\mathrm{i} = 100\,\mathrm{s}$, the size becomes uniform, and finally when $t_\mathrm{i} = 200\,\mathrm{s}$ the ordered island system is established. Therefore, in general, with increasing growth interruption time, the system ultimately reaches equilibrium.

4 QUANTUM-DOT STACKS

Having seen the effects of temperature, flux rate, surface coverage, and growth interruption time on the island formation (where only a single QD layer over the substrate is concerned), the interaction between QD layers is now studied. As before, the important contribution of the strain energy field will be emphasized.

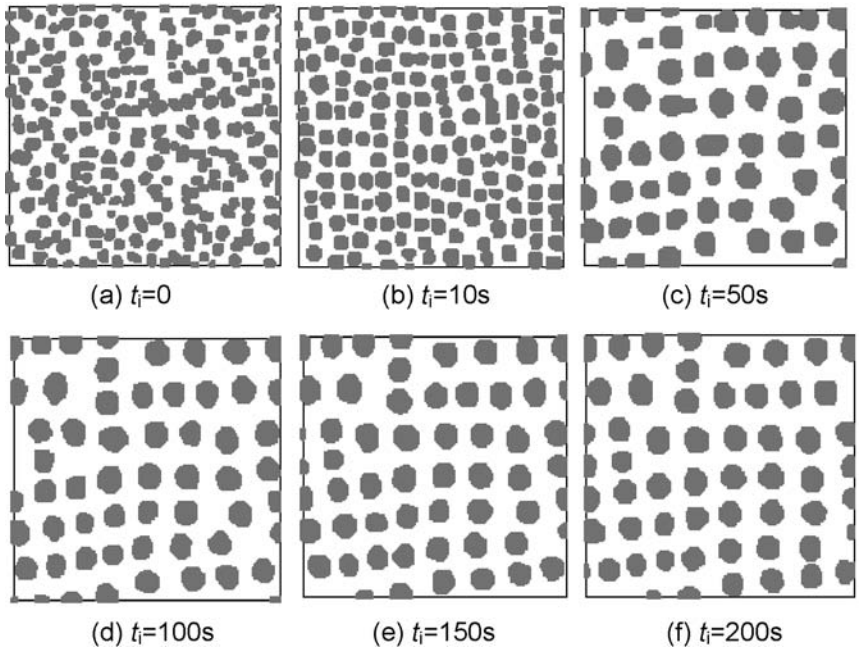

Fig. 7 Atom island distributions for different growth interruption times from $t_i = 0$ to $t_i = 200$ s in (a) to (f), where (a) is the initial atom pattern when all the atoms are deposited on the surface with growth interruption time $t_i = 0$. The simulation parameters are $T = 750$ K, $F = 1.0$ Ml/s, and $c = 20$ per cent on a 200×200 grid. The strain energy field is updated every 2500 steps

To increase the uniformity and ordering of the QD density over the surface, various approaches have been proposed, including growth of QDs over patterned substrates. Strained-layer heteroepitaxy has been studied in the lateral as well as the vertical direction [**28**–**30**]. Recently, it has been demonstrated that regular three-dimensional QD superlattices with tunable lattice constants can be achieved utilizing the strain-mediated self-organization effect in the Stranski–Krastanov growth mode [**5**, **31**].

In this section, the spatial correlation in the vertical direction is first demonstrated by simulation for a three-layered model (one substrate and two spacer layers, Fig. 8) with temperature $T = 700$ K, flux rate $F = 0.01$ Ml/s, coverage $c = 20$ per cent, growth interruption time $t_i = 50$ s (i.e. total time $t = 70$ s), and thickness for each spacer layer at $H = 5$ grids (Fig. 8). Then the thickness effect of the first spacer layer is carried out (corresponding to a two-layered model). For the first case, the simulated results on the substrate and on the first and second spacer layers are shown in Fig. 9. In this model, atoms with a pattern similar to Fig. 7(a) on the substrate GaAs (001) are first deposited. Then, KMC is executed and the simulated pattern on the substrate is shown in Fig. 9(a) (for the first QD layer). Next, a spacer layer is added of thickness $H = 5$ grids on top of the first QD layer, and again atoms are randomly deposited on the surface of this spacer layer. Similar KMC simulation is then carried out. However, when the strain energy field on the new surface (i.e. on the top of the first spacer layer) is calculated, not only the strain contribution on the surface but also that from the first QD layer (due to the previously formed atomic pattern) is considered. The simulation again runs to the interruption time $t_i = 50$ s and the result is plotted in Fig. 9(b) (for the second QD layer). Finally, following the same procedure, a new spacer layer of thickness $H = 5$ grids is added on top of the second QD layer and atoms are deposited over this spacer layer. During the simulation for this case, the strain energy at each atom location on the surface is evaluated by considering all the contributions of atoms in QD layers 1 and 2 as well as those on the surface. The simulated result is shown in Fig. 9(c) (for the third QD layer).

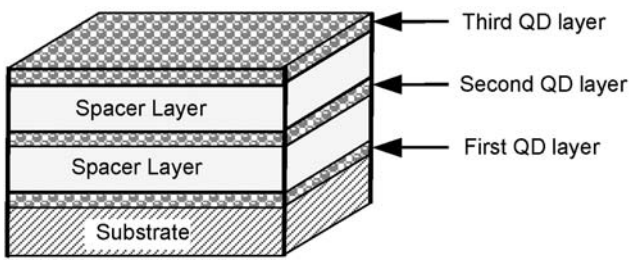

Fig. 8 Schematic illustration of a three-layered QD superlattice

It is observed from Fig. 9 that with increasing number of spacer layers the island (i.e. QD) size tends to become larger and the corresponding spatial distribution becomes more uniform [**5**, **10**, **22**]. This

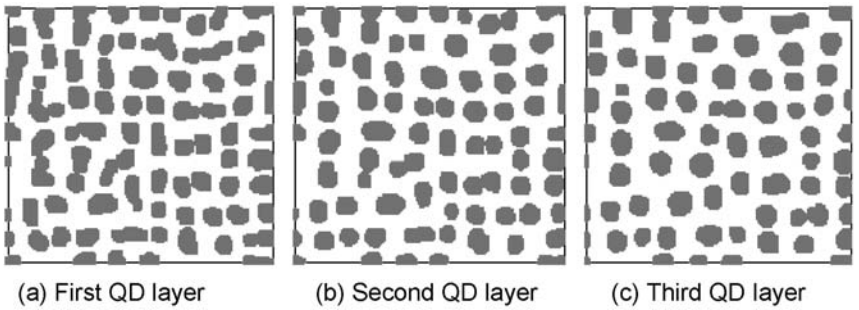

Fig. 9 QD distributions in the first (a), second (b), and third (c) QD layer (see Fig. 8 for illustration). Simulation parameters are $T = 700$ K, $F = 0.01$ Ml/s, $c = 20$ per cent, and $t = 70$ s for each layer on a 200×200 grid. Thickness of the two spacer layers is five grids each. The strain energy field is calculated every 2500 steps for each QD layer. It takes each QD layer 20 s to deposit atoms on the surface and 50 s for growth interruption

phenomenon is understandable as the strain energy distribution from the buried QDs enhances the strain on the surface so that the strain energy pattern becomes more uniform and ordered [**10**].

The effect of the thickness of the spacer (or buffer) layer on the QD distribution (a two-layered model with a substrate and a spacer layer) is now studied. The KMC program for different thicknesses of spacer layer is run, with results in Figs 10(b) to (f) corresponding to $H = 5$, 10, 15, 20, and 30 grids. While the calculation is carried out for the whole 200×200 grid, only the results within the 100×100 grid are selected to show the features. It is observed from Fig. 10 that the island size distribution over the spacer layer with thickness $H = 10$ grids is more uniform than that in the first QD layer (Figs 10(c) versus 10(a)), and that the island size distribution over the spacer layer with $H = 5$ grids is more uniform than that for $H = 10$ grids (Figs 10(b) versus 10(c)). In other words, a thinner spacer layer corresponds to a better island distribution [**22**]. Furthermore, when H is equal to, or larger than, 15 grids, no apparent ordering of islands can be observed, just as for the first QD layer case (Fig.

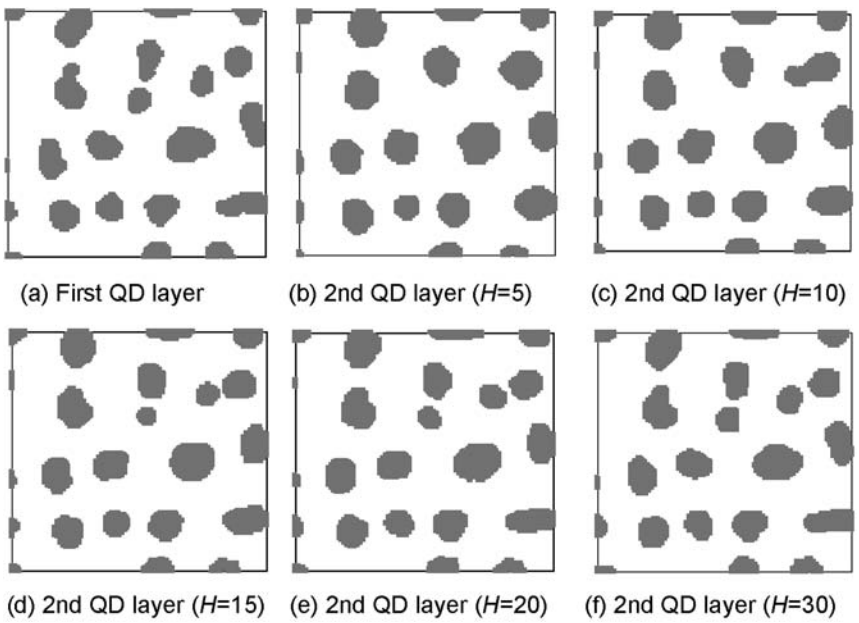

Fig. 10 QD island distributions in the second QD layer with different thicknesses for the spacer layer: (a) simulated result on top of the substrate (first QD layer); (b) to (f) simulated results on top of the spacer layer with a thickness equal to 5–30 grids (second QD layer, see also Fig. 8). The simulation parameters are $T = 700$ K, $F = 0.01$ Ml/s, $c = 20$ per cent, and $t = 70$ s for each QD layer on a 200×200 grid. The strain energy field is updated every 2500 steps. It takes each QD layer 20 s to deposit atoms on the surface and 50 s for interruption. For illustration, only the (100×100) portion of the 200×200 grid is chosen

10(a)). This is due to the fact that, when the spacer (buffer) layer is too thick, the strain energy contribution from the QDs below the spacer layer (e.g. from the first QD layer) is almost negligible as compared with the contribution from the lateral islands on the surface.

5 CONCLUSIONS

The KMC model proposed in this paper shows clearly the effect of self-organization on the dynamics of QD island growth. The nearest and next nearest neighbour binding energy may induce isolated island pattern, but neither uniform size nor spatial ordering can be observed in the absence of strain energy. The long-range strain energy field due to the lattice misfit between the substrate and adatoms is accurately evaluated based on the novel point eigenstrain Green's function solution, which could be the key factor in controlling the island size uniformity and spatial ordering. All the simulation results presented in this paper, except for the QD stacks, are limited to two-dimensional plane island growth.

Besides the long-range strain energy, other growth parameters can also greatly influence the simulation results. The average island size increases with increasing temperature up to a critical point which is around 800 K; for a temperature higher than this critical value, the islands begin to dissociate. The flux rate of atoms to the surface during deposition has a pronounced effect on the island size and ordering, which demonstrates that a large size and more uniform ordering of islands generally corresponds to a decreasing flux rate. By increasing the surface coverage, the average island size increases up to a critical point, which is somewhere between 20 and 30 per cent for the testing model; above this critical coverage, isolated islands cannot be observed. Repeated growth of QD layers in a vertical direction, separated by the thin buffer (or spacer) layer and directed by the long-range strain energy field, could be a potential way to introduce uniform island size and ordered spatial distribution.

Finally, the results presented in this paper are based on the so-called two-dimensional plane simulation. As such, the program will be able to predict only the size and spatial distribution of the islands in the horizontal (x, y) plane. To investigate the three-dimensional shape of the islands, other approaches need to be incorporated. These include the $1+1$ and $2+1$ dimension simulations where the vertical profile of the island (e.g. in the vertical (x, z) plane) can be studied [**32**]. In predicting the vertical profile of the islands [**33**], the mechanism and process become more complicated [**4**, **34**]. This topic, combined with the two-dimensional program developed, may require consideration of the Asaro–Tiller–Grinfeld morphological instability of the strained solid [**35**].

ACKNOWLEDGEMENT

This work was carried out while the first author (EP) was visiting the School of Mechanical and Production Engineering at Nanyang Technological University under the Tan Chin Tuan Exchange Fellowship in the summer of 2004. He would like to thank Prof. K. M. Liew and the School for their hospitality during his stay there. All the authors would like to thank both reviewers for their very constructive comments/suggestions.

REFERENCES

1 **Bressler-Hill, V., Varma, S., Lorke, A., Nosho, B. Z., Petroff, P. M.,** and **Weinberg, W. H.** Island scaling in strained heteroepitaxy: InAs/GaAs(001). *Phys. Rev. Lett.*, 1995, **74**, 3209–3212.

2 **Bimberg, D., Grundmann, M.,** and **Ledentsov, N. N.** *Quantum Dot Heterostructures*, 1998 (John Wiley, Chichester).

3 **Daruka, I.** and **Barabási, A.-L.** Dislocation-free island formation in heteroepitaxial growth: a study at equilibrium. *Phys. Rev. Lett.*, 1997, **79**, 3708–3711.

4 **Shchukin, V.** and **Bimberg, D.** Spontaneous ordering of nanostructures on crystal surfaces. *Rev. Mod. Phys.*, 1999, **71**, 1125–1171.

5 **Springholz, G., Pinczolits, M., Mayer, P., Holy, V., Bauer, G., Kang, H.,** and **Salamanca-Riba, L.** Tuning of vertical and lateral correlations in self-organized $PbSePb_{1-x}Eu_xTe$ quantum dot superlattices. *Phys. Rev. Lett.*, 2000, **84**, 4669–4672.

6 **Ratsch, C., Gyure, M. F., Caflisch, R. E., Gibou, F., Petersen, M., Kang, M., Garcia, J.,** and **Vvedensky, D. D.** Level-set method for island dynamics in epitaxial growth. *Phys. Rev. B*, 2002, **65**, 195 403.

7 **Meixner, M., Kunert, R.,** and **Schöll, E.** Control of strain-mediated growth kinetics of self-assembled semiconductor quantum dots. *Phys. Rev. B*, 2003, **67**, 195 301.

8 **Schöll, E.** and **Bose, S.** Kinetic Monte Carlo simulation of the nucleation stage of the self-organized growth of quantum dots. *Solid-State Electronics*, 1998, **42**, 1587–1591.

9 **Elsholz, F., Meixner, M.,** and **Schöll, E.** Kinetic Monte Carlo simulation of self-organized pattern formation in the thin film deposition. *Nuclear Inst. Meth. Phys. Res. B*, 2003, **202**, 249–254.

10 **Springholz, G., Pinczolits, M., Holy, V., Zenlauth, S., Vavra, I.,** and **Bauer, G.** Tuning of vertical and lateral correlations in self-organized $PbSePb_{1-x}Eu_xTe$ quantum dot superlattices. *Phys. E*, 2001, **9**, 149–163.

11 **Meixner, M.** and **Schöll, E.** Kinetically enhanced correlation and anticorrelation effects in self-organized quantum dot stacks. *Phys. Rev. B*, 2003, **67**, 121 202.

12 **Pan, E.** Elastic and piezoelectric fields around a quantum dot: fully coupled or semicoupled model? *J. Appl. Phys.*, 2002a, **91**, 3785–3796.
13 **Pan, E.** Elastic and piezoelectric fields in substrates GaAs (001) and GaAs (111) due to a buried quantum dot. *J. Appl. Phys.*, 2002, **91**, 6379–6387.
14 **Pan, E.** and **Yuan, F. G.** Three-dimensional Green's functions in anisotropic bimaterials. *Int. J. Solids Struct.*, 2000, **37**, 5329–5351.
15 **Shchukin, V. A., Borovkov, A. J., Ledentsov, N. N.,** and **Bimberg, D.** Tuning and breakdown of faceting under externally applied stress. *Phys. Rev. B*, 1995, **51**, 10 104–10 118.
16 **Kaminskii, A. Y.** and **Suris, R. A.** Smoothing of crystal surfaces during growth interruption. *Appl. Surf. Sci.*, 1996, **104/5**, 312–316.
17 **Schmidt, K. H., Medeiros-Ribeiro, G., Garcia, J.,** and **Petroff, P. M.** Size quantization effects in InAs self-assembled quantum dots. *Appl. Phys. Lett.*, 1997, **70**, 1727–1729.
18 **Liu, H. Y., Sellers, I. R., Gutiérrez, M., Groom, K. M., Soong, W. M., Hopkinson, M., David, J. P. R., Beanland, R., Badcock, T. J., Mowbray, D. J.,** and **Skolnick, M. S.** Influences of the spacer layer growth temperature on multilayer InAs/GaAs quantum dot structures. *J. Appl. Phys.*, 2004, **96**, 1988–1992.
19 **Ma, W. Q., Hussein, M. L., Shultz, J. L., Salamo, G. J., Mishima, T. D.,** and **Johnson, M. B.** Enhancing the in-plane spatial ordering of quantum dots. *Phys. Rev. B*, 2004, **69**, 233 312.
20 **Daruka, I., Barabási, A.-L., Zhou, S. J., Germann, T. C., Lomdahl, P. S.,** and **Bishop, A. R.** Molecular-dynamics investigation of the surface stress distribution in a Ge/Si quantum dot superlattice. *Phys. Rev. B*, 1999, **60**, R2150–R2153.
21 **Xie, Q., Chen, P.,** and **Madhukar, A.** InAs island-induced-strain driven adatom migration during GaAs overlayer growth. *Appl. Phys. Lett.*, 1994, **65**, 2051–2053.
22 **Tersoff, J., Teichert, C.,** and **Lagally, M. G.** Self-organization in growth of quantum dot superlattices. *Phys. Rev. Lett.*, 1996, **76**, 1675–1678.
23 **Shchukin, V. A., Bimberg, D., Malyshkin, V. G.,** and **Ledentsov, N. N.** Vertical correlations and anticorrelations in multisheet arrays of two-dimensional islands. *Phys. Rev. B*, 1998, **57**, 12 262–12 274.
24 **Nurminen, L., Kuronen, A.,** and **Kaski, K.** Kinetic Monte Carlo simulation of nucleation on patterned substrates. *Phys. Rev. B*, 2001, **63**, 035 407.
25 **Larsson, M.** Kinetic Monte Carlo simulations of adatom island decay on Cu(111). *Phys. Rev. B*, 2001, **64**, 115 428.
26 **Bortz, A. B., Kalos, M. H.,** and **Lebowitz, J. L.** A new algorithm for Monte Carlo simulation of Ising spin systems. *J. Comput. Phys.*, 1975, **17**, 10–18.
27 **Zhdanov, V. P.** and **Kasemo, B.** Nontraditional models of Ostwald ripening on solid surfaces: from physics to biology. *Surf. Sci.*, 1999, **437**, 307–316.
28 **Moison, J. M., Houzay, F., Barthe, F., Leprinece, L., André, E.,** and **Vatel, O.** Self-organized growth of regular nanometer-scale InAs dots on GaAs. *Appl. Phys. Lett.*, 1994, **64**, 196–198.
29 **Leonhard, D., Pond, K.,** and **Petroff, P. M.** Critical layer thickness for self-assembled InAs islands on GaAs. *Phys. Rev. B*, 1994, **50**, 11687–11692.
30 **Nötzel, R.** Self-organized growth of quantum-dot structures. *Semicond. Sci. Technol.*, 1996, **11**, 1365–1379.
31 **Lechner, R. T., Schülli, T. U., Holy, V., Stangl, J., Raab, A., Springholz, G.,** and **Bauer, G.** 3D hexagonal versus trigonal ordering in self-organized PbSe quantum dot superlattices. *Physica F*, 2004, **21**, 611–614.
32 **Schulze, T. P., Smereka, P.,** and **E, W.** Coupling kinetic Monte-Carlo and continuum models with application to epitaxial growth. *J. Comput. Phys.*, 2003, **189**, 197–211.
33 **Jacobi, K.** Atomic structure of InAs quantum dots on GaAs. *Prog. Surf. Sci.*, 2003, **71**, 185–215.
34 **Wang, L. G., Kratzer, P., Moll, N.,** and **Scheffler, M.** Size, shape, and stability of InAs quantum dots on the GaAs (001) substrate. *Phys. Rev. B*, 2000, **62**, 1897–1904.
35 **Stangl, J., Holy, V.,** and **Bauer, G.** Structural properties of self-organized semiconductor nanostructures. *Rev. Mod. Phys.*, 2004, **76**, 725–783.
36 **Tonon, F., Pan, E.,** and **Amadei, B.** Green's functions and boundary element method formulation for 3D anisotropic media. *Computers and Struct.*, 2001, **79**, 469–482.
37 **Ting, T. C. T.** *Anisotropic Elasticity: Theory and Applications*, 1996 (Oxford University Press, Oxford).
38 **Pan, E.** Mindlin's problem for an anisotropic piezoelectric half space with general boundary conditions. *Proc. R. Soc. (Lond.) A*, 2002, **458**, 181–208.

APPENDIX 1

Notation

a_j	eigenvectors
b_j	eigenvectors
c	surface coverage
C_{11}, C_{12}, C_{44}	elastic coefficients of GaAs (001)
E_{b}	binding energy of a single nearest neighbour
E_{n}	binding energy to the surface
E_{s}	total binding energy to the neighbouring atoms
$E_{\mathrm{str}}(x, y)$	strain energy
F	flux rate
g	coupling factor between adjacent lattice sites
H	spacer layer thickness
k_{B}	Boltzmann's constant
n, m	number of nearest and next nearest atoms respectively
p_{atom}	total diffusion probability of an atom
p_{j}	Stroh eigenvalue
p_{total}	probability summation of all the atoms
r	radius around the point where the strain is to be evaluated
R_{i}	cumulative probability
r_{j}	atom probability list

t	simulation time
T	temperature
t_i	growth interruption time
$\mathbf{T}(\boldsymbol{x};\boldsymbol{y}), \mathbf{S}(\boldsymbol{x};\boldsymbol{y}),$ $\mathbf{T}^{\infty}(\boldsymbol{x};\boldsymbol{y}), \mathbf{S}^{\infty}(\boldsymbol{x};\boldsymbol{y})$	Green's stress matrices
u	random number between 0 and 1
x	coordinate in the x direction
$\boldsymbol{x}$	vector for field point (x_1, x_2, x_3)
y	coordinate in the y direction
$\boldsymbol{y}$	vector for source point $(\mathbf{y}_1, \mathbf{y}_2, \mathbf{y}_3)$
α	reduction factor for the next nearest neighbours $(= 1/\sqrt{2})$
γ_{ij}	strain tensor
γ^*_{ij}	misfit strain (or eigenstrain)
Δt	time step
ν_0	attempt frequency
σ_{ij}	stress tensor

APPENDIX 2

Half-space Green's function and elastic strain energy

In this appendix, the Green's function in an anisotropic and linearly elastic half-space under traction-free surface condition (Fig. 11) [**14**], is first briefly reviewed and then applied to the calculation of the elastic strain energy in atom islands. The half-space Green's function is expressed as the sum of the full-space Green's function and a complementary part. While the full-space Green's function is in an explicit analytical form [**36**], the complementary part is expressed in terms of a regular line integral that can be easily evaluated by a standard quadrature scheme.

It is observed from equation (5) that the misfit lattice γ^*_{lm}-induced strain can be expressed as a combination of the derivatives of the stresses due to a point force, while the point force (in the j direction) induced strain is just γ^j_{kp}. Therefore, the induced strains due to a point eigenstrain and a point force are completely different and should be carefully distinguished, even though the former can be expressed by the latter (via derivatives)! To calculate the lattice misfit induced strain, the derivatives of the point force induced stresses are needed with respect to the source coordinate $\boldsymbol{y}$, which can be expressed as [**14**]

$$\frac{\partial \mathbf{T}(\boldsymbol{x};\boldsymbol{y})}{\partial y_j} = \frac{\partial \mathbf{T}^{\infty}(\boldsymbol{x};\boldsymbol{y})}{\partial y_j} - \frac{1}{2\pi^2}\int_0^{\pi} \bar{\mathbf{B}}\mathbf{G}_3\langle g_j\rangle \mathbf{A}^T \,\mathrm{d}\theta$$
$$\frac{\partial \mathbf{S}(\boldsymbol{x};\boldsymbol{y})}{\partial y_j} = \frac{\partial \mathbf{S}^{\infty}(\boldsymbol{x};\boldsymbol{y})}{\partial y_j} - \frac{1}{2\pi^2}\int_0^{\pi} \bar{\mathbf{C}}\mathbf{G}_3\langle g_j\rangle \mathbf{A}^T \,\mathrm{d}\theta \tag{7}$$

where an over bar stands for a complex conjugate while superscript 'T' denotes the matrix transpose. The definitions of Green's **T** and **S** matrices are given as

$$\mathbf{T} = \begin{bmatrix} \sigma^1_{31} & \sigma^2_{31} & \sigma^3_{31} \\ \sigma^1_{32} & \sigma^2_{32} & \sigma^3_{32} \\ \sigma^1_{33} & \sigma^2_{33} & \sigma^3_{33} \end{bmatrix}, \qquad \mathbf{S} = \begin{bmatrix} \sigma^1_{11} & \sigma^2_{11} & \sigma^3_{11} \\ \sigma^1_{12} & \sigma^2_{12} & \sigma^3_{12} \\ \sigma^1_{22} & \sigma^2_{22} & \sigma^3_{22} \end{bmatrix} \tag{8}$$

with $\mathbf{T}^{\infty}(\boldsymbol{x};\boldsymbol{y})$ and $\mathbf{S}^{\infty}(\boldsymbol{x};\boldsymbol{y})$ corresponding to the full-space counterparts. Also, in equation (7)

$$\langle g_1\rangle = \mathrm{diag}[\cos\theta,\ \cos\theta,\ \cos\theta]$$
$$\langle g_2\rangle = \mathrm{diag}[\sin\theta,\ \sin\theta,\ \sin\theta]$$
$$\langle g_3\rangle = \mathrm{diag}[p_1(\theta), p_2(\theta), p_3(\theta)] \tag{9}$$

$$(\mathbf{G}_3)_{ij} = \frac{(\bar{\mathbf{B}}^{-1}(\theta)\mathbf{B}(\theta))_{ij}}{\{-\bar{p}_i(\theta)x_3 + p_j(\theta)y_3 - [(x_1 - y_1)\cos\theta + (x_2 - y_2)\sin\theta]\}^3} \tag{10}$$

with $p_i(\theta)$ being the Stroh eigenvalues and $\mathbf{A}(\theta)$, $\mathbf{B}(\theta)$ the corresponding eigenmatrices, while matrix $\mathbf{C}(\theta)$ is related to $\mathbf{A}(\theta)$ [**37**]. Note that all these eigenvalues and matrices are functions of the stiffness matrix $\mathbf{C}_{ijkl}$ and the integral variable θ [**14**, **37**, **38**].

As has been presented in the text, with equation (5), the interactive strain energy at point $\boldsymbol{y}$ of island **B** due to neighbouring island **A** (Fig. 12) can be expressed as an integration, given in equation (6) and repeated below for convenience

$$E_{\mathrm{str}}(\boldsymbol{y}) = \frac{1}{2}C_{ijkl}\iint_A \gamma_{ij}(\boldsymbol{y};\boldsymbol{x})\gamma_{kl}(\boldsymbol{y};\boldsymbol{x})\,\mathrm{d}A(\boldsymbol{x}) \tag{11}$$

The integration of equation (11) on the right-hand side can be approximated by the summation of n

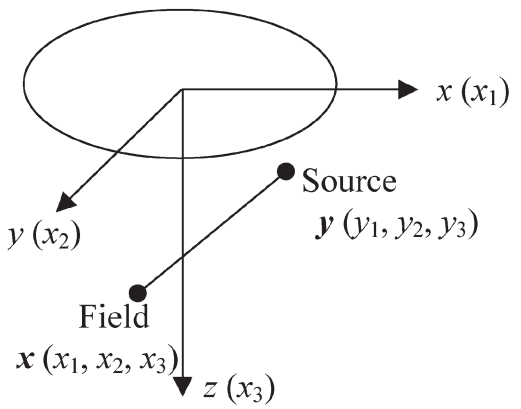

Fig. 11 Geometry of the half-space Green's function with the source point at $\boldsymbol{y}(y_1, y_2, y_3)$ and the field point at $\boldsymbol{x}(x_1, x_2, x_3)$

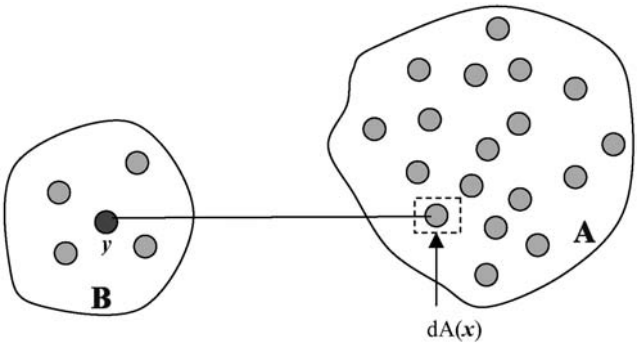

Fig. 12 Illustration of the interactive strain energy among atoms. The strain energy at the atom point y of island **B** due to island **A** is the integration over the atom area of island **A**

discretized areas over the island **A** as

$$E_{\text{str}}(\boldsymbol{y}) = \frac{1}{2} C_{ijkl} \sum_n \gamma_{ij}(\boldsymbol{y}; \boldsymbol{x}_n)\gamma_{kl}(\boldsymbol{y}; \boldsymbol{x}_n)\Delta A_n \qquad (12)$$

Since the Green's functions have been precalculated, each ΔA in equation (12) can be very small. It actually can be small enough to include only one atom. In other words, if there are N atoms in island **A** with coordinate $\boldsymbol{x}_n$, then the induced strain energy at $\boldsymbol{y}$ in island **B** can be finally expressed simply as (assuming that each atom has the same mass m)

$$E_{\text{str}}(\boldsymbol{y}) = \frac{1}{2} C_{ijkl} m \sum_{n=1}^{N} \gamma_{ij}(\boldsymbol{y}; \boldsymbol{x}_n)\gamma_{kl}(\boldsymbol{y}; \boldsymbol{x}_n) \qquad (13)$$

APPENDIX 3

Detailed simulation steps

1. Set simulation time $t = 0$ and hopping step $= 0$.
2. Randomly grow seeds in the lattice grid, for example, 20 per cent of the total atoms.
3. Extend the original area using a periodic condition (Fig. 13).
4. Judge the number and position of nearest and next nearest neighbours for each atom, and judge the position for each atom in the second box (Fig. 14). This information is used to calculate the overall binding energy E_{n} (equation 4).
5. Calculate the probability for each atom, and, if the hopping step reaches 2500, update the strain energy field. After that, set the hopping step back to 0.

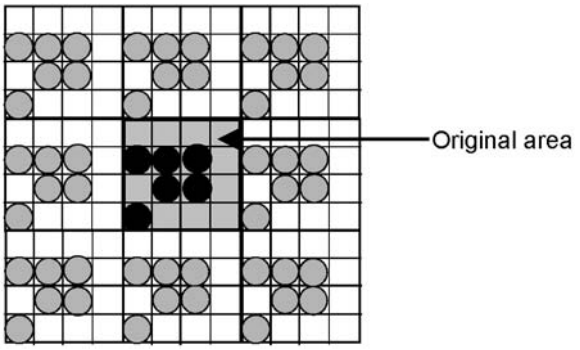

Fig. 13 Illustration of the periodic boundary condition

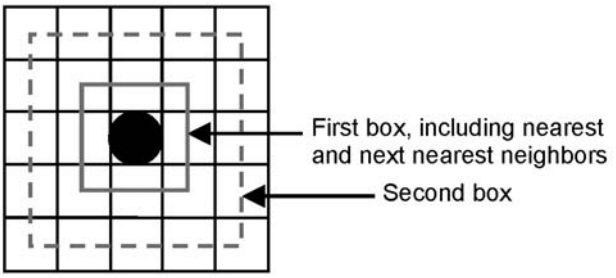

Fig. 14 Illustration of the atom neighbours

6. Form a list of $r_j = p_{\text{atom}}[j]$ (probability) and calculate the cumulative function

$$R_i = \sum_{j=1}^{i} r_j \qquad \text{for } i = 1, 2, \ldots, N \qquad (14)$$

   where N is the total number of atoms in the system.
7. Take a random number $u \in [0, 1)$.
8. Find the ith atom and carry out the hopping according to the value R_i, for which $R_{i-1} < uR \leqslant R_i$, where R is the total probability p_{total}.
9. Make a jump for the atom in accordance with the likelihood of the eight possible diffusion processes.
10. Update the time by $t = t + \Delta t$, where

$$\Delta t = -\log u / R \qquad (15)$$

11. Update the total hopping step.
12. Update the jumping probability of each atom and each class.
13. Return to step 3.